

High Energy Gain and Transverse Instability in Three-Dimensional Simulations of Light Sail Acceleration

A. Sgattoni,^{1,2,*} S. Sinigardi,^{2,3,4} and A. Macchi^{2,5}

¹*Dipartimento di Energia, Politecnico di Milano, Milano, Italy*

²*Istituto Nazionale di Ottica, Consiglio Nazionale delle Ricerche, research unit “Adriano Gozzini”, Pisa, Italy*

³*Dipartimento di Fisica e Astronomia, Università di Bologna, via Irnerio 46, 40126 Bologna, Italy*

⁴*INFN sezione di Bologna, viale Berti Pichat 6/2, 40127 Bologna, Italy*

⁵*Dipartimento di Fisica “Enrico Fermi”, Università di Pisa, Largo Bruno Pontecorvo 3, I-56127 Pisa, Italy*

(Dated: November 16, 2019)

The dynamics of radiation pressure acceleration in the light sail regime are analysed by means of large scale, three-dimensional (3D) particle-in-cell simulations. Considering thin and dense plasma targets with an optimal areal density and ultra-intense laser pulses with irradiance values $> 10^{22}$ W cm⁻² μm², the target quickly reaches relativistic velocities and, differently to other mechanisms, the 3D dynamics leads to faster and higher energy gain than in 1D or 2D geometry. This effect is caused by the local decrease of the target density due to transverse expansion leading to a “lighter sail”. A fast rising instability, observed and characterized for the first time in 3D simulations, leads to strong transverse modulation of the accelerated ion beam.

The development of high power laser systems able to deliver short ultraintense-pulses drove an increasing interest to study laser-plasma interaction with particular focus on realizing compact sources of high energy electrons, ions and photons. In particular, several mechanisms of ion acceleration have been proposed and tested [1, 2] also thanks to progress in target manufacturing [3] and pulse contrast [4]. These latter allowed the first recent experimental investigations of radiation pressure acceleration (RPA) of thin solid foils, i.e. the so-called light sail (LS) regime [5–7]. On the theoretical side, the LS configuration has been proposed and studied in the last ten years and it has been shown through simulations [8] that LS becomes very efficient at intensities beyond 10^{23} W cm⁻² (foreseen with next generation facilities) in the regime where the ions become relativistic.

In the basic one-dimensional (1D) picture of LS, the target behaves almost as a perfect mirror and can be accelerated to relativistic velocities $V = \beta c$ with an efficiency $\eta = 2\beta/(1+\beta)$ that asymptotically tends to unity, provided that the target integrity and its reflectivity are kept on a sufficiently long time scale. The energy gain, though, after an early stage of exponential growth, becomes rather slow ($\gamma(t) \sim t^{1/3}$ where $\gamma = (1 - \beta^2)^{-1/2}$) opening issues in a realistic three-dimensional (3D) scenario where the acceleration length required to obtain the maximum energy (for a given laser pulse) may exceed the Rayleigh length of the laser beam. However, it has been theoretically shown [9] that, in proper conditions and in a multidimensional case where the laser pulse has a finite focal spot, the decrease of the target areal density due to transverse expansion may lead to a faster energy gain, $\gamma(t) \sim t^{3/5}$ in 3D geometry. The target becomes progressively “lighter” and “unlimited” energy gain is predicted, although at the expense of the number of accelerated ions.

As an additional issue, some experimental evidence

have been found of transverse Rayleigh-Taylor-like instabilities [6] which may be a cause of early breakthrough of the laser pulse and inefficient acceleration. Theoretical modeling [10, 11] has shown the growth rate to increase monotonously with the instability wavevector, similarly to the classic hydrodynamic instability.

The RPA-LS regime has been so far investigated extensively with particle-in-cell (PIC) simulations mostly in 1D and 2D (see e.g. Refs.[9, 12]), with few 3D studies having been performed [8, 13–15] mainly due to the very demanding computational requests. Since the scaling of ion energy with time, the diffraction length of the laser pulse and the dynamics of instabilities are all dependent on the dimensionality of the system, a comprehensive 3D investigation on long time scales is essential. A previous numerical work [13] brought preliminary evidence of ion energies being higher in 3D than in lower dimensionality, but for computational reasons the simulations did not reach the end of the acceleration stage.

Here we present the results of large scale 3D simulations performed with the PIC code ALaDyn [16]. We followed the LS dynamics in the ultrarelativistic regime until the end of the acceleration stage. We observed that in 3D the energy gain of the fastest ions is higher and faster than in 1D and 2D, and that the evolution of the maximum ion energy with time follows the power laws predicted by the analytical theory of Ref.[9]. Peculiar net-like structures in the ion density were observed in the plane perpendicular to the acceleration direction and attributed to the 3D dynamics of a transverse instability. This instability does not prevent the acceleration to continue after the early formation of the structures and a good laminarity of the ion beam to be maintained. The “unlimited” acceleration is however limited by the onset of the target transparency.

The 3D simulations of Ref.[13] indicated an “operating point”, defined by the use of circular polarization

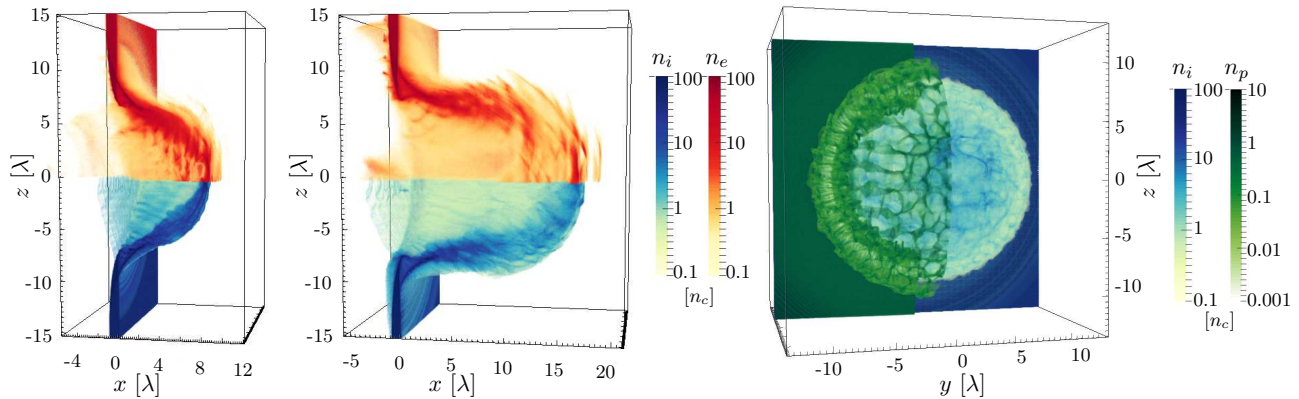


FIG. 1. Left ($t = 20T$) and central ($t = 30T$) panel: 3D snapshots of the density of electrons (red tones, upper half, $z > 0$) and Carbon ions (blue tones, lower half, $z < 0$). Only the $y > 0$ region is shown for visualization purposes. Right panel: snapshot at $t = 30T$ from a different perspective, showing the densities of Carbon ions (for $|y| \leq 15$ and $|z| \leq 15$, blue tones) and of protons (for $-15 \leq y \leq 0$ and $|z| \leq 15$, green tones).

(CP) of the laser pulse and by the target thickness ℓ_t matching the laser amplitude $\zeta = \pi(n_e/n_c)(\ell_t/\lambda) \simeq a_0$ ($a_0 = (I/2m_e c^3 n_c)^{1/2}$, where I is the laser intensity) which yields the highest ion energy while being relatively unaffected by both limited numerical resolution and inclusion of radiation friction effects. In order to extend the simulations on a much longer time scale we use a lower number of particles per cell after having verified that using the same parameters the results of Ref.[13] are unaffected. In addition, we employed a non uniform grid in the transverse direction: a constant cell spacing was maintained in a region around the axis and then gradually stretched (using the tangent as stretching function) towards the edge. This allowed us to keep a high resolution in the center and contain the expanding plasma with a reasonable number of grid points. The simulation box was 93λ wide along x (the laser-propagation direction) and 120λ along y and z . In the central region the transverse resolution was $\Delta y = \Delta z = \lambda/22$. The grid size was $4096 \times 1792 \times 1792$ cells and we used 64 macro particles per cell per species accounting for a total number of about 2×10^{10} in the whole simulation. The simulations were run on the FERMI BlueGene/Q machine of the CINECA supercomputing facility (Bologna, Italy) using 16384 cores.

In the following we mostly focus on a target composed of a first layer of ions with charge to mass ratio $Z/A = 1/2$ (e.g. C^{6+}), thickness $\ell_t = \lambda$ (with λ the laser wavelength) and initial electron density $n_e = 64n_c$ (with $n_c = \pi m_e c^2 / e^2 \lambda^2$ the critical density), and a second layer of protons, thickness $\ell_r = \lambda/22$ and density $n_e = 8n_c$. For reasons of computational feasibility, the density is lower than for real solid targets (for comparison Carbon targets have a mean electron density around $400n_c$) but the areal density has a realistic value (for Diamond-like Carbon foils the thickness may be down

to $\lambda/100$). The target configuration mimics a solid foil with impurities on the rear side and allows to differentiate the dynamics of different charge states. The peak normalized amplitude of the laser field corresponding to the “optimal” thickness condition $a_0 \simeq \zeta$ is $a_0 = 198$. In all simulations, the laser pulse has a transverse Gaussian profile with waist diameter $w = 6\lambda$ and a longitudinal \cos^2 -like profile with a FWHM duration $\tau_p = 9T$ (where $T = \lambda/c$ is the laser period), all referred to the profile of the fields. The simulations have been run for a time $t = 80T$, where $t = 0$ corresponds to the moment when the laser pulse front reaches the edge of the target.

Fig.1 shows density snapshots for both electrons and ions at intermediate stages of the acceleration process for a simulation with optimal amplitude $a_0 = 198$. The side view shows the strong typical “cocoon” deformation of the target. The electron density shows structures imprinted by the laser fields with longitudinal modulation on the scale of λ , similar to those observed in Refs.[13, 14]. A front view reveals a transverse, net-like structuring of the ion density, which is rather evident in the protons.

First we discuss the ion energy spectra at the end of the simulation of Fig.1. As we are primarily interested in ions moving near the axis we select particles whose momentum is within a cone with a semi aperture of 5 degrees. Inside this cone, the proton spectrum has a narrow peak, while the Carbon distribution is broad as shown in Fig.2 (a). The maximum energy per nucleon of carbon ions and protons are identical indicating that the most energetic particles of both species move at the same velocity, which is a typical feature of idealized LS. In contrast, for a 3D simulation identical to that of Fig.1 but with linear polarization (LP) instead of CP (and the peak field amplitude $a_0 = 198\sqrt{2} \simeq 280$ to keep the same mean intensity), the ions with different Z/A ratio tend

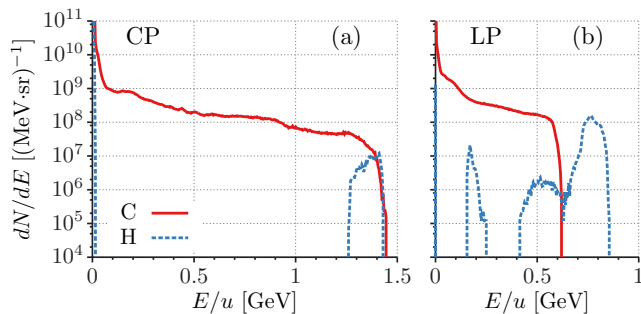


FIG. 2. Energy spectra for carbon ions (solid red line) and protons (dashed blue line) at the end ($t = 80T$) of the simulations with circular (CP, left) and linear (LP, right) polarization, for ions within a cone with semi-aperture 5 of degrees around the x -axis. The absolute numbers in $\text{MeV}^{-1}\text{sr}^{-1}$ have been obtained assuming $\lambda = 0.8\mu\text{m}$.

to form separate bands in the energy spectra, with the protons ending up with highest energy and the cut-off for heavier ions being in correspondence of the lower end of the proton peak, as shown in Fig.2 (b). This behavior is also observed in simulations at lower intensity ($a_0 = 100$), both for CP and LP. Similar features were also found experimentally at much lower intensities [7].

Being $\sigma_y, \sigma p_y, m_y$ respectively variance of y p_y and covariance of (y, p_y) , we calculated the transverse RMS emittance $\epsilon_y = (\sigma_y \sigma p_y - m_y^2)^{1/2}$ of the ions having energy per nucleon $E > 500\text{MeV}/u$ (for the conversion to physical units we assume $\lambda = 0.8\mu\text{m}$) obtaining for the carbon ions $\epsilon_y \simeq \epsilon_z = 4 \times 10^{-2}$ mm mrad. Similarly, for protons, we got $\epsilon_y \simeq \epsilon_z = 8 \times 10^{-2}$ mm mrad. These emittance values are very small, thanks to the microscopic spot size, but the comparison with values from conventional accelerators is difficult due to the non-monochromaticity of the ion and proton bunches. Nonetheless, the numbers are compatible with experimental results on laser-driven acceleration at much lower intensities and proton energies [17].

We now consider the evolution of the cut-off energy of Carbon ions with time, shown in Fig.3 (a). Data for both the 3D simulation of Figs.1-2 and a 2D simulation with the same parameters are shown. In both cases, after an early stage of exponential growth ($t \lesssim 8T$) the time evolution shows an intermediate stage where the time dependence is well fitted by a power law function (see below) until the acceleration saturates. Analysis of the simulations shows that such transition occurs when the target becomes transparent to the laser pulse. In the 3D case the energy rises with time faster than in 2D but the transition to transparency is also reached at an earlier time. Eventually the final energy values in 2D and 3D are very close, but both much higher than the 1D value. The cut-off energy of protons from the “contaminant” layer follows the temporal history of the energy of C ions

closely. Notice that the energy of both H and C ions shows some “oscillations” around the mean value, both in 3D as shown in Fig.3 (b) and 2D. Such oscillations are related to lighter ions getting higher acceleration from the longitudinal field in the early stages overtaking the heavier ions, which however causes the acceleration of lighter ions to stop because of the evanescence of the fields due to screening by the layer of heavier ions which, in turn, overtake the lighter ions again. As a result the same energy for both species is reached only asymptotically.

For the intermediate stage we used a power law $m_p c^2 \gamma(t) = k_D (t - t_0)^{\alpha_D}$ as fitting function with three free parameters (k_D, t_0, α_D). The values of α_D are in very good agreement with the predictions of the analytical model of Ref.[9], which we hereby summarize. The basic idea of the model comes from considering a target areal density dependent upon time $\sigma(t) = \sigma_0 / \Lambda^{D-1}(t)$ being $\Lambda(t)$ a function describing the local dilation of the target (according to $r_\perp(t) = \Lambda(t)r_\perp(0)$ in Lagrangian coordinates) and $D = 1, 2, 3$ the dimensionality of the system. It is assumed that for ions the transverse motion is ballistic with constant transverse momentum after an initial “kick”. An analytical estimate can be obtained considering the effect of the transverse ponderomotive force of a Gaussian laser pulse, $dp_\perp/dt \simeq -m_e c^2 \partial_r \sqrt{1 + a^2(r)}$, where $\langle a^2(r) \rangle = a_0^2 \exp(-2r^2/w^2)$. Near the focal axis ($r \ll w$) we have $dp_\perp/dt \simeq m_e c^2 2r/w$ and thus, considering an impulsive acceleration on a time Δt , we obtain

$$p_\perp \simeq m_e c^2 \frac{2r(0)}{w^2} a_0 \Delta t \equiv m_p r(0) \bar{\omega}_0, \quad (1)$$

where $\bar{\omega}_0$ is thus a parameter depending on the initial kick. The transverse velocity decreases as a result of the increase in the longitudinal momentum p_\parallel , and assuming $p_\perp \ll p_\parallel = m_p c \gamma(t)$ we obtain $d\Lambda/dt = \bar{\omega}_0 / \gamma(t)$. This latter equation is coupled to the one describing the LS motion with variable surface density, $d(\gamma\beta)/dt = \Omega \Lambda^{D-1}(t) (1 - \beta)/(1 + \beta)$ with $\Omega = 2I/\sigma_0 c^2$. The solution is easy to obtain for a constant intensity and in the asymptotic, strongly relativistic limit for which $\beta \rightarrow 1$, $(1 - \beta)/(1 + \beta) \rightarrow 1/4\gamma^2$:

$$\gamma(t) = \left(\frac{t}{\tau_D} \right)^\alpha, \quad \alpha = \frac{D}{D+2} \quad (2)$$

where the time constants τ_D are

$$\tau_1 = \left(\frac{3}{4\Omega} \right), \quad \tau_2 = \left(\frac{1}{\Omega \bar{\omega}_0} \right)^{1/2}, \quad \tau_3 = \left(\frac{48}{125\Omega \bar{\omega}_0^2} \right)^{1/3}. \quad (3)$$

The parameters obtained from the fit of Fig.3 thus allow to obtain the value of $\bar{\omega}_0$, obtaining $\bar{\omega}_0 \simeq 2.8 \times 10^{-2}$ in the 3D case and $\bar{\omega}_0 \simeq 1.4 \times 10^{-2}$ in 2D. The analytical estimate based on Eq.(1) gives $\bar{\omega}_0 \simeq (2m_e/m_p)(a_0/w^2)\Delta t \simeq 6 \times 10^{-3}(\Delta t/T)$ which matches the simulation result if $\Delta t \simeq 4.7T$.

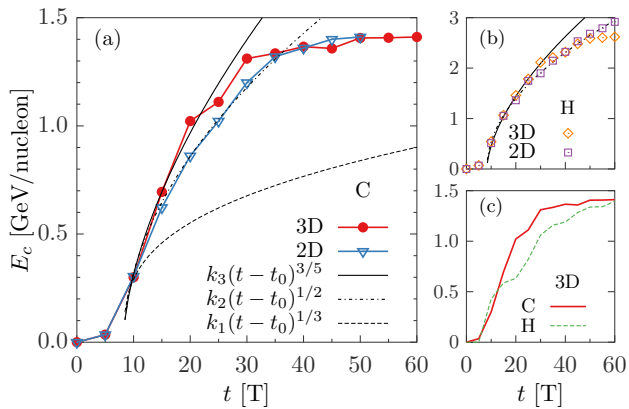


FIG. 3. (a): cut-off energy (GeV) of C ions for the 3D simulation of Fig.1 (red circles) and a 2D simulation with same parameters (blue triangles). The continuous and dash-dotted line represent the fits with power law functions ($k_3 = 220$ and $k_2 = 245$). A similar function with the predicted 1D scaling is drawn for comparison with a dashed line. (b): same as (a), but for a pure hydrogen target ($k_3 = 330$ and $k_2 = 410$). (c) comparison between the energy of C ions and of protons in 3D for the same simulation of (a).

Simulations were also performed with a slab of hydrogen plasma $Z = A = 1$ as in Refs.[8, 13], all other parameters being equal to Fig. 1. As shown in Fig.3 (c) the energy still follows closely the analytical scaling, reaching higher energies due to the lighter target; the values for the $\bar{\omega}_0$ parameters are 5.5×10^{-2} and 5.7×10^{-2} for the 3D and the 2D case, respectively. However, we notice that in the 2D case the scaling is followed for all the simulation time and the final energy is higher than for the 3D case. For the latter, the extra dimension allows a faster expansion which “boosts” the acceleration, but also leads to an earlier onset of transparency. Looking at the density distribution we observe that the transition to transparency occurs when the peak value is about $10n_c$.

We now discuss the formation of net-like structures in the density of ions, both for C ions and for protons, already apparent in Fig.1. In Fig.4 we show the ion areal density on the transverse plane y, z at $t = 60T$, considering only the particles with kinetic energy $E > 500\text{MeV/u}$. For both C^{+6} and H^+ , the “net-like” like pattern is visible; in particular the protons exhibit both a very strong modulation and a denser region in the form of spiral, which is likely to be an imprint of the CP pulse. The simulations for LP also shows a net-like modulation with no spiral and a tendency of the structures to lengthen along the polarization direction. A “synthetic image” (not shown) of both protons and C ions obtained projecting the trajectories of the numerical particles on a plane orthogonal to the laser axis, shows very similar features. Such image would correspond to what would be observed, assuming ballistic propagation, on the plane of a detector such as a radiochromic film as in Ref.[6].

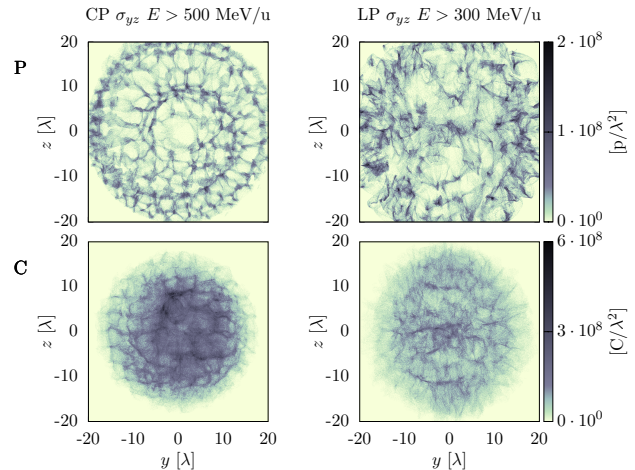


FIG. 4. Areal density of protons (P) and carbon (C) ions having energy $> 500\text{MeV/u}$, obtained by projection of the y, x plane at time $t = 60T$, from the 3D simulation with circular polarization (CP) of Fig.1 and the corresponding simulation with linear polarization (LP).

The transverse structures are already visible at $t \simeq 10T$, thus their growth do not prevent to reach relativistic ion energies and to preserve low emittances. At the end of the simulation the typical transverse scale of the instability is of the order of λ or smaller (to gain confidence that such scale is not affected by “numerical imprinting”, due to the periodicity of either the grid or the domain decomposition in the transverse direction, we performed simulations with some initial temperature and found no difference). As a model for the instability growth which is complementary to those presented in Refs.[10, 11], here we discuss the possible role of the modulation of the radiation pressure at a rippled interface. We take as a simple example the incidence of a monochromatic plane wave of (complex) amplitude $\mathbf{E}_0 = E_0 \hat{z}$ on a mirror surface described by the curve $x = \delta \cos(qy)$. For $q > k = 2\pi/\lambda$ and in the limit $\delta \ll \lambda$, the magnetic field at the surface has components $B_y \simeq E_0[2 + \kappa_1 \delta \cos(qy)]$, where $\kappa_1 = (q^2 - k^2)^{1/2}$, and $B_x \simeq E_0 q \delta \sin(qy)$. This yields a modulated radiation pressure $P_{\text{rad}} \simeq (E_0^2/2\pi)[1 + \kappa_1 \delta \cos(qy)]$, which is thus stronger in the dips of the modulation and would tend to make it deeper. However, as the modulation depth δ becomes comparable to λ , if $q > 2k$ the electromagnetic field may not penetrate anymore, similarly to what happens in a waveguide. Qualitatively, this would account for the instability to saturate at a transverse wavevector $q \simeq (2/\lambda)$, similarly to what is observed in the simulations. The fact that the structures appear to be a bit larger than $\lambda/2$ may be ascribed to relativistic increase of the pulse wavelength in the sail frame.

In conclusion, three-dimensional simulations of light sail acceleration in the relativistic regime show that the

energy gain versus time is much faster than in a one-dimensional model and show a scaling in very good agreement with the analytical theory of Refs.[9]. The energy gain, however, is interrupted by the onset of target transparency which takes place earlier in 3D than in 2D, counterbalancing the effect of faster rarefaction. A transverse instability develops already in the initial stage of acceleration and the resulting structures in the ion beam profiles have been characterized for both circular and linear polarization. The possibility of optical modulation effects playing a role in the instability onset and saturation has been outlined. These findings are highly relevant to the design of next generation facilities for laser-driven ion acceleration at ultra-relativistic intensity.

We acknowledge PRACE for access to the BlueGene/Q “FERMI”, based in Italy at CINECA, via the project “LSAIL”. Support from MIUR, Italy, via the FIR project “SULDIS” is also acknowledged.

* andrea.sgattoni@polimi.it

- [1] A. Macchi, M. Borghesi, and M. Passoni, *Rev. Mod. Phys.* **85**, 751 (2013).
- [2] H. Daido, M. Nishiuchi, and A. S. Pirozhkov, *Rep. Prog. Phys.* **75**, 056401 (2012).
- [3] W. Ma, V. Liechtenstein, J. Szerypo, D. Jung, P. Hilz, B. Hegelich, H. Maier, J. Schreiber, and D. Habs, *Nucl. Inst. Meth. Phys. Res. A* **655**, 53 (2011).
- [4] B. Dromey, S. Kar, M. Zepf, and P. Foster, *Rev. Scient. Instr.* **75**, 645 (2004); C. Thaury *et al.*, *Nat. Phys.* **3**, 424 (2007).
- [5] A. Henig *et al.*, *Phys. Rev. Lett.* **103**, 245003 (2009); F. Dollar *et al.*, *ibid.* **108**, 175005 (2012); I. J. Kim *et al.*, *ibid.* **111**, 165003 (2013); B. Aurand *et al.*, *New J. Phys.* **15**, 033031 (2013); S. Steinke *et al.*, *Phys. Rev. ST Accel. Beams* **16**, 011303 (2013).
- [6] C. A. J. Palmer *et al.*, *Phys. Rev. Lett.* **108**, 225002 (2012).
- [7] S. Kar *et al.*, *Phys. Rev. Lett.* **109**, 185006 (2012).
- [8] T. Esirkepov, M. Borghesi, S. V. Bulanov, G. Mourou, and T. Tajima, *Phys. Rev. Lett.* **92**, 175003 (2004).
- [9] S. V. Bulanov, E. Y. Echkina, T. Z. Esirkepov, I. N. Inovenkov, M. Kando, F. Pegoraro, and G. Korn, *Phys. Rev. Lett.* **104**, 135003 (2010); *Phys. Plasmas* **17**, 063102 (2010).
- [10] F. Pegoraro and S. V. Bulanov, *Phys. Rev. Lett.* **99**, 065002 (2007).
- [11] V. Khudik, S. A. Yi, C. Siemon, and G. Shvets, *Phys. Plasmas* **21**, 013110 (2014).
- [12] O. Klimo, J. Psikal, J. Limpouch, and V. T. Tikhonchuk, *Phys. Rev. ST Accel. Beams* **11**, 031301 (2008); A. P. L. Robinson, M. Zepf, S. Kar, R. G. Evans, and C. Bellei, *New J. Phys.* **10**, 013021 (2008); A. Macchi, S. Veghini, T. V. Liseykina, and F. Pegoraro, **12**, 045013 (2010); X. Q. Yan, H. C. Wu, Z. M. Sheng, J. E. Chen, and J. Meyer-ter-Vehn, *Phys. Rev. Lett.* **103**, 135001 (2009); B. Qiao, M. Zepf, M. Borghesi, B. Dromey, M. Geissler, A. Karmakar, and P. Gibbon, **105**, 155002 (2010).
- [13] M. Tamburini, T. V. Liseykina, F. Pegoraro, and A. Macchi, *Phys. Rev. E* **85**, 016407 (2012).
- [14] T.-P. Yu, A. Pukhov, Z.-M. Sheng, F. Liu, and G. Shvets, *Phys. Rev. Lett.* **110**, 045001 (2013).
- [15] H. Xu *et al.*, *Appl. Phys. Lett.* **104**, 024105 (2014).
- [16] C. Benedetti, A. Sgattoni, G. Turchetti, and P. Londrillo, *IEEE Transaction on Plasma Science* **36**, 1790 (2008); P. Londrillo, C. Benedetti, A. Sgattoni, and G. Turchetti, *Nucl. Inst. Meth. Phys. Res. A* **620**, 28 (2010).
- [17] T. E. Cowan *et al.*, *Phys. Rev. Lett.* **92**, 204801 (2004); F. Nuernberg *et al.*, *Rev. Sci. Instrum.* **80**, 033301 (2009).